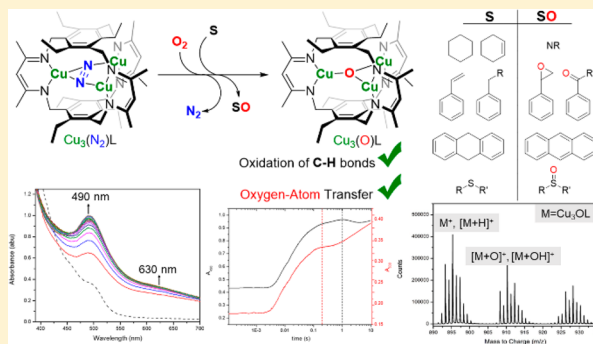


A Tricopper(I) Complex Competent for O Atom Transfer, C–H Bond Activation, and Multiple O₂ Activation StepsBrian J. Cook,^{†,§} Gianna N. Di Francesco,^{†,§} Matthew T. Kieber-Emmons,^{‡,§} and Leslie J. Murray^{*,†,§}[†]Center for Catalysis and Florida Center for Heterocyclic Compounds, Department of Chemistry, University of Florida, Gainesville, Florida 32611-7200, United States[‡]Department of Chemistry, University of Utah, Salt Lake City, Utah 84112-0850, United States

S Supporting Information

ABSTRACT: Oxygenation of a tricopper(I) cyclophanate (**1**) affords reactive transients competent for C–H bond activation and O atom transfer to various substrates (including toluene, dihydroanthracene, and ethylmethylsulfide) based on ¹H NMR, gas chromatography/mass spectrometry (MS), and electrospray ionization (ESI)/MS data. Low product yields (<1%) are determined for C–H activation substrates (e.g., toluene, ethylbenzene), which we attribute to competitive ligand oxidation. The combined stopped-flow UV/visible, electron paramagnetic resonance, ESI/MS, ¹H NMR, and density functional theory (DFT) results for reaction of **1** with O₂ are consistent with transient peroxy- and di(μ-oxo)-bridged intermediates. DFT calculations elucidate a concerted proton-coupled electron transfer from toluene to the di(μ-oxo) intermediate and subsequent radical rebound as the C–H activation mechanism. Our results support a multicopper oxidase-like mechanism for O₂ activation by **1**, traversing species similar to the coplanar Cu₃O₂ unit in the peroxy and native intermediates.



■ INTRODUCTION

Dioxygen activation by multicopper oxidases (MCOs) couple dioxygen reduction to water with a number biochemical processes, including substrate oxidation and selective ion transport.^{1,2} The diverse reactivity of copper–dioxygen adducts arising from similar active-site structures has inspired ongoing work to replicate this reactivity in model compounds. In particular, the potential for copper complexes to function as catalysts for C–H bond functionalization and dioxygen reduction have applications in green synthesis and in fuel cells.³ The tricopper(I) state of MCOs is proposed to react with O₂ to arrest at a peroxide-bridged transient (PI) and requires a further one e[−]/H⁺ reduction to complete O₂ bond scission to yield the native intermediate (NI; Figure 1).^{1a,5} Contrastingly, no synthetic tricopper–dioxygen adduct arrests at the peroxide state, although stable peroxy–dicopper(II) species and those in equilibrium in the di(μ-oxo) congeners have precedent (Figure 1).⁷ These tricopper compounds are capable of H atom abstraction from substrates (e.g., phenols) or O atom transfer to phosphines. Density functional theory (DFT) studies on MCOs indicates that O₂ binds coplanar with the Cu₃ plane, whereas the O–O vector is orthogonal to the Cu₃ plane in model compounds.^{5,6d,8}

The consequence of O₂ orientation relative to the metal centers on bond activation remains poorly understood. Our hypothesis is that the orientation of the O₂ fragment relative to the tricopper plane is a key element differentiating the reactivity

of reported model compounds from that of the enzymatic systems. With this consideration in mind, the steric constraints imposed by our cyclophane ligand can likely enforce the desired coplanar orientation of O₂ binding. To that end, we report the oxygenation of a Cu₃^I cyclophanate, **1**, in which the macrobicyclic enforces an MCO-like O₂ coordination to the metal ions.^{2a,3b,6b,d,9} Oxygenated transients **1**•O₂ are competent for C–H activation of C–H bonds of substrates such as 9,10-dihydroanthracene and toluene and O atom transfer to styrene and ethylmethyl sulfide. DFT calculations on this system point to a covalent [Cu₃(μ₃-O)(μ₂-O)]³⁺ cluster as one likely reactive intermediate. These in silico studies point to a favorable H atom abstraction from PhMe followed by radical rebound to afford the alcohol product. In addition, the initial metal complex product of O atom transfer is identified as a μ₃-oxotricopper(II/II/I) complex, which can react with an additional equivalent of O₂. Our results highlight the importance of O₂ orientation as a key factor in dictating the reactivity of multimetallic species.

■ EXPERIMENTAL SECTION

General Considerations. All reactions were prepared under a dinitrogen atmosphere in an Innovative Technologies glovebox and then transferred to a Schlenk line. Unless otherwise explicitly stated, all

Received: April 5, 2018

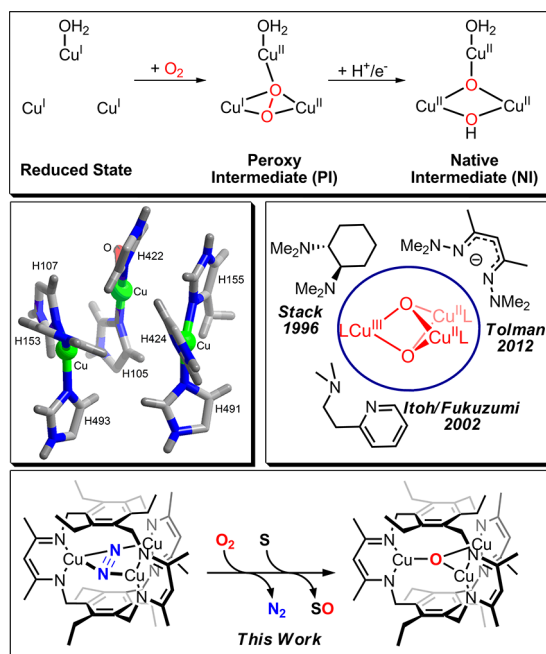


Figure 1. Proposed mechanism for O_2 reduction by multicopper oxidases traverses peroxo- and a $(\mu\text{-hydroxo})(\mu_3\text{-oxo})$ tricopper transients abbreviated PI and NI (top).¹ The active site of laccase from *Steccherinum murashkinskyi* (PDB ID: 5MIB) with Cu ions depicted as green spheres and the proteinaceous ligands as sticks (bottom, left). Crystallographically characterized di($\mu_3\text{-oxo}$)tricopper compounds synthesized by reaction of monocopper(I) complexes of the depicted ligands and dioxygen.^{4,6}

solvents and reagents were purchased from Sigma-Aldrich. Solvents were dried using an Innovative Technologies solvent purification system and stored over activated 3 Å molecular sieves inside the dinitrogen-filled glovebox. Ultra High Purity (UHP) O_2 was purchased from AirGas. Deuterated solvents were purchased from Cambridge Isotope Laboratories (CIL) and purified according to reported procedures for the proteo-solvents and then stored over activated 3 Å molecular sieves under inert atmosphere.¹⁰ NMR spectra were collected on a Varian Inova operating at 500 MHz for ^1H , equipped with a three-channel 5 mm indirect detection probe with z-axis gradients. All chemical shifts are reported in parts per million and referenced to tetramethylsilane for ^1H . Electrospray ionization (ESI) mass spectrometry (MS) was conducted in positive mode by direct injection using a manual injector, which fed into a constant flow of anhydrous air-free solvent, and then into an Agilent 6120 TOF spectrometer. The following ESI and MS conditions were used: gas temperature = 350 °C and fragmentation voltage = 120 V. Gas chromatography (GC) analyses were conducted using a Varian CP-3800 gas chromatogram using a flame ionization detector (FID) and equipped with a J&W Scientific DB-35MS capillary column, 0.5 μm , 30 m \times 0.53 mm. Samples were run on a Thermo Scientific Trace DSQ GC-MS in EI mode using a 30 m Stabilwax-DA column using a temperature profile starting with a hold at 50 °C for 2 min followed by a ramp to 175 °C at 6°/min and then a second temperature ramp to 250 °C at 15°/min. Retention times were measured for the substrates and potential oxidation products using commercially available compounds and loaded on to the GC column with a 10:1 split and a 0.1 μL (90 mM in tetrahydrofuran (THF)) sample injection. $[\text{H}(\text{DMF})][\text{OTf}]$ (DMF = dimethylformamide) was prepared as described previously.¹¹ Deuterated 9,10-dihydroanthracene ($d_4\text{-DHA}$), the ligand H_3L , and tricopper complex **1**, were synthesized as reported previously.^{9b,c,12}

Stopped-Flow UV/Visible Spectroscopy. Experiments were performed with a TgK Scientific CSF-61DX2 cryogenic stopped-flow instrument in single-mixing mode using the Kinetic Studio v.4 software

package. All accessories were supplied by TgK Scientific. Absorbance measurements were conducted with a Xe or quartz–tungsten lamp with either a diode array (multiwavelength data) or a photomultiplier (single wavelength data) detector. In addition to the solvent drying procedure reported above, solvents used in these experiments were also stirred over NaK for 24 h prior to use. Instrument lines were rinsed with a dilute solution of sodium benzophenone ketyl in THF and then extensively with anhydrous and anaerobic THF or *n*-hexane. Solutions of $1\cdot\text{N}_2$ in THF (1.1 mM) or **1'** in *n*-hexane (0.66 mM) were prepared in the glovebox and then loaded onto the stopped-flow instrument using gastight syringes (Hamilton Laboratory Products). Dioxygen-saturated THF and *n*-hexane were prepared by vigorously sparging an aliquot of the particular solvent (~ 15 mL) for 30 min with UHP O_2 on a vacuum/inert gas manifold, and the O_2 -saturated solvent was then transferred to the stopped-flow instrument using Hamilton gastight syringes. Data were collected at -80 °C for *n*-hexanes, and the spectra were fit using a three-exponential, four-component kinetic model as described elsewhere.¹³ For the 490 nm single-wavelength data set, data were truncated to 4 ms–1.0 s for fitting purposes to account for instrument dead time and downstream decay products, which could not be fit reliably. For the 630 nm single-wavelength data set, data were truncated to 4–200 ms for fitting purposes to account for instrument dead time and downstream decay products.

EPR Spectroscopy. A solution of $1\cdot\text{N}_2$ in toluene (1.5 mM, ~ 1 mL) was transferred to a quartz tube inside of a dinitrogen-filled glovebox. The tube was capped with a Teflon valve, removed from the glovebox, and placed under N_2 on a vacuum manifold. The solution was then degassed by three freeze–pump–thaw cycles, after which the tube was placed in $\text{CO}_2(\text{s})$ /isopropanol bath. After the sample had thawed under vacuum, tube was refilled with O_2 and then flash frozen after ~ 10 s using liquid nitrogen. The sample tube was then evacuated, flame-sealed, and stored at 77 K. Electron paramagnetic resonance (EPR) spectra were collected on a Bruker Elexsys E580 with a Bruker 4116DM resonator maintained at 5 K with a liquid helium-cooled cryostat. Data were collected in perpendicular mode from 50 to 7050 G with the following parameters: power = 0.633 mW; frequency = 9.407 GHz; modulation frequency = 100.00 kHz; modulation amplitude = 10.00 G; and gain = 60 dB. In parallel mode, from 50 to 7050 G with the following parameters: power = 2.00 mW; frequency = 9.410 GHz; modulation frequency = 100.00 kHz; modulation amplitude = 10.00 G; and gain = 60 dB.

Synthesis of 2. In a typical synthesis, 35.0 mg (0.0391 mmol) of Cu_3OL ³⁵ was dissolved in 10 mL of THF and added to a 50 mL round-bottom Schlenk flask with a Teflon screw-cap seal valve. This was attached to a Schlenk line and degassed with three consecutive freeze–pump–thaw cycles to remove dissolved gases. The flask was then backfilled with UHP O_2 and allowed to thaw to room temperature. The reaction was allowed to stir vigorously for 30 min under static O_2 , which resulted in a color change from dark yellow to dark maroon. After this color change was complete, volatiles were removed from the reaction vessel under reduced pressure to yield the final product as a dark purple solid. ^1H NMR (300 MHz, $\text{THF}-d_6$, 298 K): δ (ppm), 129.0(br, 12H), $-18.4(\text{s}, 18\text{H})$, $-30.9(\text{s}, 3\text{H})$. Other ligand-derived signals could not be reasonably assigned. Attenuated total reflectance (ATR) IR (cm^{-1}): 2959(m), 2925(m), 2868(m), 1550(s), 1522(m), 1469(m), 1434(s), 1405(vs), 1373(m), 1331(m), 1237(w), 1066(w), 1014(w), 730(m).

H_2O_2 Quantification by Iodometric Titration. Adapted from a previously reported procedure.²⁶ Under N_2 , 15.8 mg (0.0174 mmol) of $1\cdot\text{N}_2$ was dissolved in 50 mL of $\text{C}_6\text{H}_5\text{F}$ (concentration = 0.349 mM), and 9.0 mg (0.0101 mmol) of **2** was dissolved in 25 mL of $\text{C}_6\text{H}_5\text{F}$ (0.407 mM). These were then transferred 20 mL scintillation vials were fitted with 14/20 rubber septa containing 5 mL of solution each. For $1\cdot\text{N}_2$, a Schlenk line connected to UHP O_2 was purged for 5 min to replace atmosphere. Under positive pressure of O_2 , each septum seal was pierced with a needle to allow O_2 flow, which caused an immediate color change from pale orange to brown. After 5 s, 1.0 mL of 17.5 mM $[\text{H}(\text{DMF})]\text{OTf}$ in MeCN was used to quench, bringing the total volume to 6.0 mL, for a final analyte concentration of 0.291 mM ($1\cdot\text{N}_2$) and 0.336 mM (**2**). The final reaction mixture

was then freeze-pumped-thawed once more. The reaction mixture (0.2 mL) was added to a 1 cm quartz cuvette, and to this was added 1.8 mL of a 0.3 M NaI solution in MeCN, for a final concentration of 0.0291 mM $\text{Cu}_3(\text{N}_2)_\text{L}$. Since $1\cdot\text{N}_2$ has a ligand-based absorption that overlaps with I_3^- ($\lambda_{\text{max}} = 361 \text{ nm}$, $\epsilon = 22\,000 \text{ M}^{-1} \text{ cm}^{-1}$), a control of $1\cdot\text{N}_2 + \text{O}_2 + [\text{H}(\text{DMF})]\text{OTf}$ was used as a background (see Figures S42 and S43). From the five trials, a total of $94.5 \pm 14.8\%$ ($1\cdot\text{N}_2$) and $52.3 \pm 9.5\%$ (2) yield of H_2O_2 .

Oxidation of Hydrocarbons and Ether. To a solid portion of $1\cdot\text{N}_2$ (0.028 mmol, 25 mg) in a 20 mL vial was added an aliquot of a THF solution of either styrene (1.6 mL, 0.87 M), toluene (1.5 mL, 0.94 M), ethylbenzene (1.7 mL, 0.82 M), diethyl ether (1.4 mL, 0.95 M), hexanes (1.8 mL, 0.80 M), cyclohexane (1.5 mL, 0.94 M), or cyclohexene (28 μL , 0.055 M). This solution was then diluted with THF to give a final reaction volume of 3 mL with concentrations of 9.2 mM for $1\cdot\text{N}_2$ and 460 mM for the given substrate. The vial was sealed with a septum and removed from the glovebox. UHP dioxygen was then introduced to the headspace of the vial for $\sim 5 \text{ s}$. The reaction was then removed from the manifold and stirred overnight under a static atmosphere, after which the reaction was opened to air, filtered through diatomaceous earth, and the filtrate was used for GC/MS measurements. Oxidation reactions using $^{18}\text{O}_2$ were prepared as described above. Reaction mixtures were injected splitless with either a 0.5 or 1 μL sample injection volume for UHP O_2 or $^{18}\text{O}_2$, respectively.

Oxidation of Ethylmethylsulfide and 9,10-Dihydroanthracene. A 50 mL pear-shaped Schlenk flask equipped with a poly(tetrafluoroethylene) (PTFE)-coated magnetic stir bar was charged with $1\cdot\text{N}_2$ (25 mg, 0.028 mmol), and either ethylmethylsulfide (0.5 mL, 5.53 mmol)/0.5 mL of THF, 9,10-dihydroanthracene (DHA; 73 mg, 0.40 mmol)/1.0 mL of THF, or d_4 -DHA (31 mg, 0.17 mmol)/1.0 mL of THF. Naphthalene was included as a gas chromatography (GC) internal standard (14.1 mg, 0.11 mmol). The flask was then removed from the glovebox and placed under Ar on a vacuum manifold. The reaction mixture was degassed by repeated freeze-pump-thaw cycles and cooled to -78°C ($\text{CO}_2/\text{isopropanol}$). The flask was then filled with 1 atm of UHP oxygen gas or $^{18}\text{O}_2$, and the vessel remained under a static atmosphere at -78°C for 15 min. An aliquot was removed and then injected into the ESI/MS instrument. After the aliquot was removed and with the temperature maintained at -78°C , all volatiles from the reaction flask were removed under reduced pressure, which required $\sim 20 \text{ min}$. The solid residue was transferred to the glovebox, and ^1H NMR spectra were recorded in either *d*-toluene or *d*-dichloromethane.

Computational Methods. Density functional theory (DFT) calculations were performed in Gaussian09 Version D.01.¹⁵ A model of the dinitrogen complex **1** was built from crystallographic coordinates and optimized as the neutral singlet with the BP86 functional. Ahlrich's triple- ζ basis set with polarization (tzvp)¹⁶ was used on Cu, O, and N atoms, and split valence with polarization (svp)¹⁷ was used on C and H atoms. The oxygenated products and reaction trajectory were computed analogously. Analytical frequency calculations were performed on all complexes to ensure stationary points on the potential energy surface had been reached, and no imaginary frequencies were found. Single-point energy calculations were performed with the b3lyp functional¹⁸ within the unrestricted formalism with an ultrafine integration grid as implemented in Gaussian09. These single-point calculations included solvation using the polarizable continuum model with the solvent parameters of THF. The overall Gibbs free energy was determined as the sum of the solvated b3lyp SCF energy and the thermal corrections from the analytical frequency calculations. Mulliken populations were determined using QMForge,¹⁹ and molecular orbitals were visualized with Lumo.²⁰

RESULTS AND DISCUSSION

Monitoring reaction of $1\cdot\text{N}_2$ with O_2 in THF at -78°C by stopped-flow (SF) UV/visible spectroscopy, we observe an initial rapid decay at $\lambda_{\text{max}} = 505 \text{ nm}$ ($<100 \text{ ms}$) followed by absorption increases at $\lambda_{\text{max}} = 490$ and 630 nm (Figures S1 and S2). ΔA_{505} may arise from N_2 dissociation, and those at 490

and 630 nm are consistent with reported Cu_nO_2 species.^{14,21} A_{430} and A_{630} kinetic traces were complex, and we were unable to simulate the data with two- or three-sequential elementary step mechanisms. We then re-examined this reaction using **1** synthesized under Ar (**1'**), which lacks the 505 nm band of $1\cdot\text{N}_2$, to better resolve ΔA_{490} and ΔA_{630} (Figures S3, S5, and S7). **1'** can be quantitatively converted to $1\cdot\text{N}_2$ upon exposure to N_2 , supporting **1'** as Cu_3L (Figures S3 and S4). Reaction of **1'** with O_2 in *n*-hexane at -80°C results in similar increases in A_{490} and A_{630} as with $1\cdot\text{N}_2$ (Figure 2). A_{430} and A_{630} data are best modeled using an $\text{A} \rightarrow \text{B} \rightarrow \text{C} \rightarrow \text{D}$ scheme (Figure 2 inset and Figures S7–S12). The employed model is consistent with the profiles of A_{630} versus A_{490} (specifically, the initial maximization time for A_{630} differs from that for A_{490}). As a caveat, however, the initial 0.28 absorption change within the instrument dead time, and the gradual persistent absorption

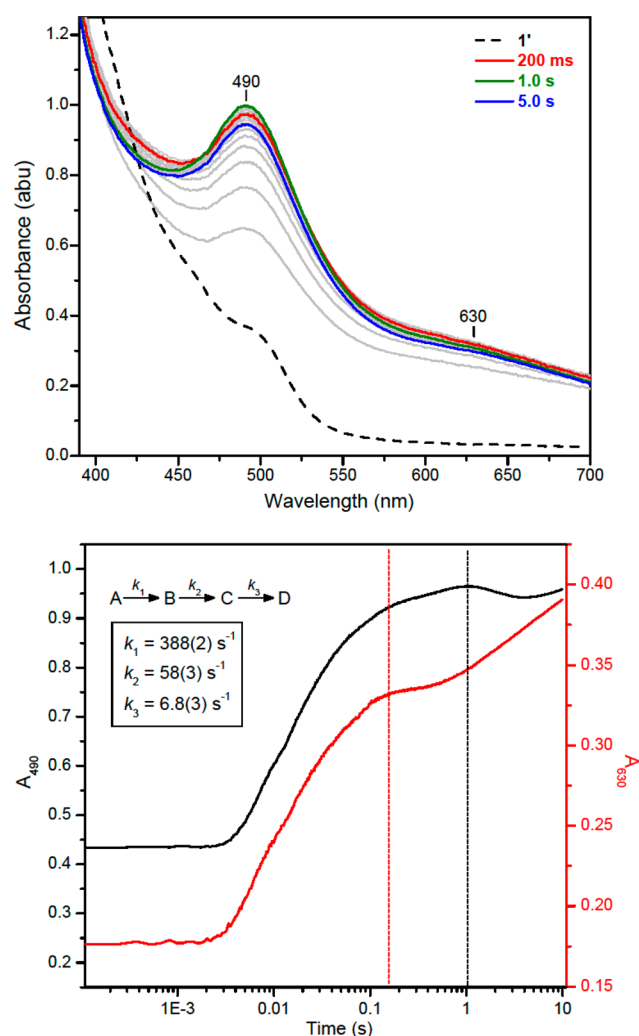


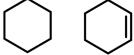
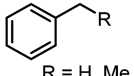
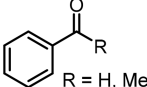
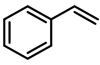
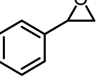
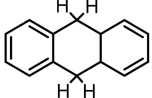
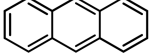
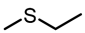
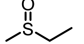
Figure 2. Stopped-flow UV/visible absorption data for reaction of 0.33 mM **1'** in *n*-hexane with O_2 -saturated *n*-hexane at -80°C monitored by diode array (top) and at 490 and 630 nm only (bottom). A rapid increase in absorption is observed within the instrument dead time considering the spectrum of the compound in the absence of O_2 (---, top) and the first spectrum collected after mixing. A_{630} has an initial maximum evident at $\sim 200 \text{ ms}$ (vertical red dashed line), whereas A_{490} maximizes at $\sim 1.0 \text{ s}$ (vertical black dashed line). Both A_{490} and A_{630} are well-modeled with a sequential three-step kinetic model over the 4–1000 ms time domain.

increases out to long reaction times (>40 min) required truncation of the data sets (4 ms–1.0 s). Our absorption maxima are comparable to ligand-to-metal charge-transfer bands at 480 nm reported for PI and Chan's tricopper-dioxygen intermediate(s).^{3c,5a,22} Our A_{490} and A_{630} data agree with reported spectral differences between peroxo- and di(μ -oxo)-dicopper compounds.^{21a,b,23} Thus, we tentatively assign B, C, and D as an initial O_2 adduct, a peroxo-bridged transient, and a di(μ -oxo)tricopper cluster, respectively. To evaluate if simpler reaction outcomes could be achieved (e.g., a stable infinite absorption value), product mixtures from reaction of $1 \cdot N_2$ with 1 equiv of O_2 were examined by 1H NMR spectroscopy, revealing three products, two of which are as-yet-identified: Cu_3OL ,³⁵ a diamagnetic C_{2v} symmetric species, and a paramagnetic product (Figure S36).

Attempts to probe the O–O bond order spectroscopically for $1 \cdot O_2$ species were unsuccessful. Absorptions assignable to O–O stretching modes for a peroxide transient were unobservable by stopped-flow infrared (SF-IR) or in Raman spectra on frozen samples using $^{16}O_2$ or $^{18}O_2$. We note that vibrational data on PI have not been reported, albeit due to protein absorption and fluorescence.²⁴ X-band EPR spectra recorded on $1 \cdot O_2$ revealed absorptions at 3244 G and ~ 1570 G in perpendicular and parallel mode (Figure S13). These spectra are comparable to those for triplet di(μ -oxo)tricopper(II/II/III) clusters.^{6d,a,25} However, the intensity ratio of the half-field versus the $g \approx 2$ signals for $1 \cdot O_2$ is significantly smaller than previously reported. We speculate that this discrepancy arises from di- and tricopper decomposition products (e.g., ligand oxidation) present in the reaction mixture, which agrees with MS data (vide infra). Finally, the H_2O_2 content of oxygenated samples of $1 \cdot N_2$ measured using the iodometric method was $95 \pm 15\%$ (Figure S42).²⁶ Taken together, these results support O_2 activation by $1 \cdot N_2$ to the peroxide, if not more reduced states.

We subsequently probed the reactivity pattern of $1 \cdot O_2$ transients. GC data on oxygenated mixtures of $1 \cdot N_2$ solutions premixed with various substrates evidenced O atom transfer (OAT) and C–H activation, albeit in low yield (Table 1,

Table 1. Yields of Oxidation Products

Substrate	Product	Yield ^a (%)
	none detected	-
 R = H, Me	 R = H, Me	H = 0.46 ^b Me = 0.46 ^b
		0.50 ^b
		1.6 ^c
		56 ^b

^aOn the basis of $[1 \cdot N_2]$. ^bDetermined by GC. ^cDetermined by 1H NMR.

Figures S14–S17). Similar carbonyl products have been observed for oxidation of the relevant substrates and attributed to overoxidation or rearrangement under reaction or GC conditions.²⁷ The low yields are expected, as oxidation of ligand benzylic positions is likely competitive with hydrocarbon oxidation. Consistently, the product yield improves substantially for the more readily oxidized EtSMe. We attempted to characterize ligand products in the absence of substrates but observed intractable complex mixtures by GC/MS and 1H NMR (Figures S29 and S30). MS data on products from reactions of $1 \cdot N_2$ and styrene or toluene using $^{18}O_2$ were shifted by 2 mass units, confirming that the incorporated O atom is O_2 -derived (Figures S18–S21). Scrambling of the ^{18}O label is observed in the products, but similar results are reported for other copper and related systems.²⁸ Oxidation products were not observed with cyclohexane, hexane, pentane, or diethyl ether as the substrates.

Thus, we estimate the oxidizing power of $1 \cdot O_2$ intermediates as 88.5 kcal/mol (bond dissociation energy (BDE) of $PhCH_3$), although the expected competitive ligand oxidation complicates this analysis.²⁹ For DHA oxidation, the predominant ion envelopes in ESI/MS data are well-simulated to a mixture of $[Cu_3O_2L+H]^+$ and $[Cu_3O_2L+2H]^+$ (Figure S32), and anthracene was observed by 1H NMR (Figure S31). If d_4 -DHA is used, resonances for d_2 -anthracene and a parent ion consistent with $[Cu_3O_2L+D]^+$, which suggests H atom abstraction (HAA), are observed in the product mixtures by 1H NMR and ESI/MS, respectively (Figures S35 and S34). This result, however, is not unambiguous, as the mass is within 5 ppm of that for $[Cu_3O_2L+2H]^+$. For EtSMe oxidation, ions corresponding to $[Cu_3O_2L]^+$, $[Cu_3O_2L+H]^+$, $[Cu_3OL]^+$, $[Cu_3OL+H]^+$, and $[EtS(O)Me+M]^+$ ($M = Li^+, Na^+, K^+$) were observed in ESI/MS data (Figures 3 and S26). An ion

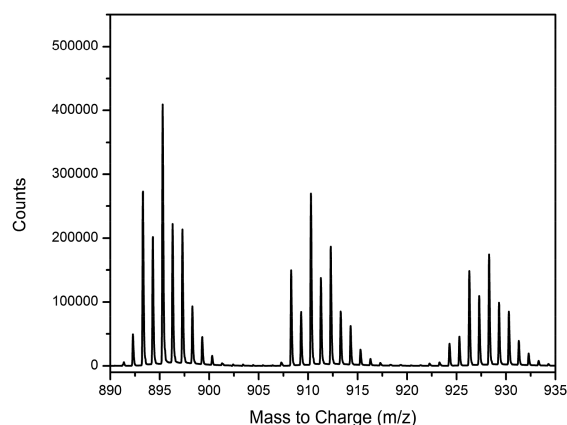


Figure 3. High-resolution ESI/MS(+) data from the oxygenation reaction of $1 \cdot N_2$ in the presence of EtSMe. Each isotopic pattern is best simulated as a combination of $[M]^+$ and $[M+H]^+$ with $m/z = 895.3047$ assigned to $[Cu_3OL]^+$ and $[Cu_3OL+H]^+$, $m/z = 910.2942$ as $[Cu_3O_2L]^+$ and $[Cu_3O_2L+H]^+$, and $m/z = 928.3004$ as $[Cu_3O_2L+H_2O]^+$ and $[Cu_3O_2L+H_3O]^+$.

envelope consistent with a dicopper species is also assignable; however, similar envelopes are also present in MS data for other purified tricopper complexes,^{9a,35} suggesting potential demetalation under analysis conditions. Using $^{18}O_2$ for EtSMe oxidation affords ions with m/z values consistent with $[Cu_3^{16/18}OL]^+$ and $[Cu_3^{16/18}OL+H]^+$, and $[Cu_3^{16/18}O_2L]^+$ and $[Cu_3^{16/18}O_2L+H]^+$. Similar to our GC/MS results, incorpo-

ration of the O atom label is also not nearly quantitative for the copper products; the cause of this scrambling remains under investigation. Resonances corresponding to Cu_3OL are also evident in ^1H NMR spectra of EtSMe and DHA oxidation reactions (Figures S24, S25, and S31).³⁵ We conclude then that **1** exhibits mono-oxygenase-like reactivity leading to C–H bond activation and OAT as potential reaction pathways.

Given the complexity of our reaction kinetics, we challenged our assumption that Cu_3OL is a terminal product of O_2 activation by **1**. Cu_3OL does not effect OAT (e.g., Me_3P) and is unreactive toward O atom donors (e.g., PhIO). Exposure of a d_8 -THF solution of Cu_3OL to O_2 at -78°C results in complete consumption of Cu_3OL to yield a paramagnetic species, **2** ($\lambda_{\text{max}} = 488\text{ nm}$, Figure S39). **2** is unstable under an O_2 atmosphere, precipitating a brown solid after $\sim 2\text{ h}$ (Figure S40), but it can be isolated if the reaction is degassed. Oxidation products are identifiable in ^1H NMR spectra of reactions of isolated **2** with DHA (Figure S45) but are undetected for reactions with toluene, ethylbenzene, or styrene. Assuming quantitative conversion of Cu_3OL to **2**, the H_2O_2 yield of 52(10)% by iodometric titration on samples of **2** (Figure S43) hint at a peroxo-bridged bis[Cu_3OL] species analogous to our bis(triiron) compound.^{12b} Another possible formula assignment for **2** is superoxo-adduct of Cu_3OL , which cannot be excluded by our data. Taken together, **1** can react with multiple equivalents of O_2 in the presence of substrates. To our knowledge, the ability of the product cluster of a mono-oxygenase reaction to react with dioxygen in the absence of additional reducing equivalents is unprecedented.

Geometry optimization of a dinitrogen-for-dioxygen substituted $1\cdot\text{N}_2$ affords two stationary points: a peroxotricopper(I/II/II) species (**3**) at -18.1 kcal/mol and a (μ -oxo)(μ_3 -oxo)tricopper(II/III/III) intermediate (**4**) at -22.9 kcal/mol (Figure 4). Notably, the Cu_3O_2 is planar in both **3** and **4**, as

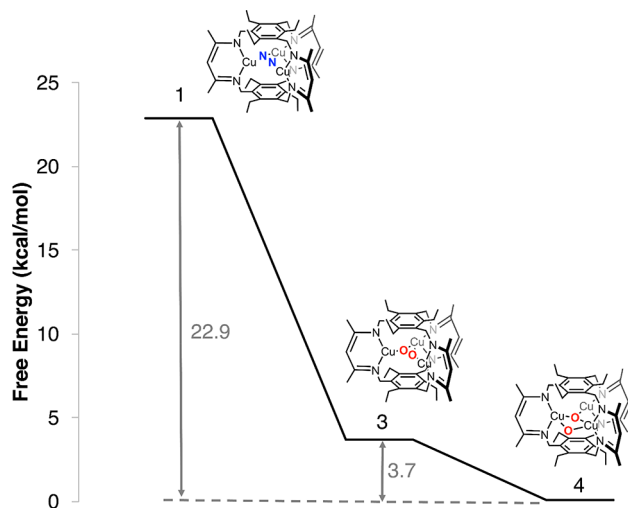


Figure 4. Reaction profile for **1** with O_2 . N_2 dissociation and O_2 coordination are favored, leading to a peroxo- (**3**) and a di(μ -oxo)-tricopper intermediates (**4**).

proposed for PI. The calculated energy separations between the $S = 0$ and 1 states of **3** and **4** (namely, $^1\mathbf{3}$, $^3\mathbf{3}$, $^1\mathbf{4}$, $^3\mathbf{4}$) are small, suggesting an equilibrium mixture, and are consistent with complexity of the kinetic data above. These results are evocative of reversible O–O bond cleavage in dicopper–dioxygen adducts—a known pathological case for energetics by DFT—

implying that geometric and electronic structures are reliable, whereas the relative thermodynamics between species should be used with caution.³⁰

The relatively short O–O distance of 1.45 \AA in **3** reflects minimal back-bonding from the unique Cu(II) ion into the O_2 σ^* orbital as is typically observed in side-on adducts to Cu. Consequently, this orbital, which would be the acceptor orbital for potential H atom abstraction, is unactivated, as the O_2 σ^* orbital is high in energy. Analysis of the unoccupied orbitals of $^3\mathbf{4}$ —the lower energy isomer of **4**—revealed a highly covalent $[\text{Cu}_3\text{O}_2]^{3+}$ core (Table S3), with three copper-based orbitals (241α , 240β , and 241β) and an unoccupied O orbital on the μ_2 -O donor (62.0% O, Figure 5). This unoccupied predom-

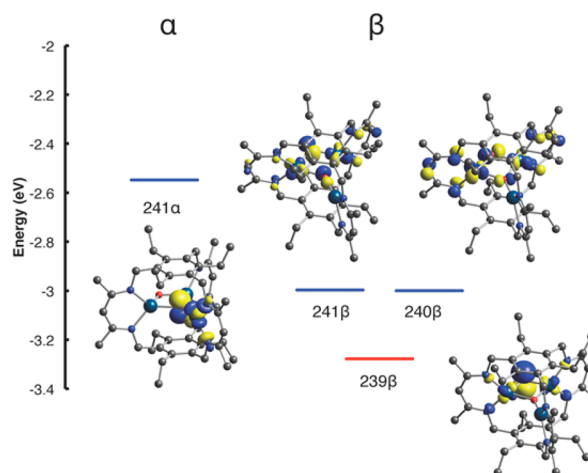


Figure 5. Unoccupied frontier molecular orbitals of **4**. The orbital depicted as a red line is comprised of significant out-of-plane radical O p character.

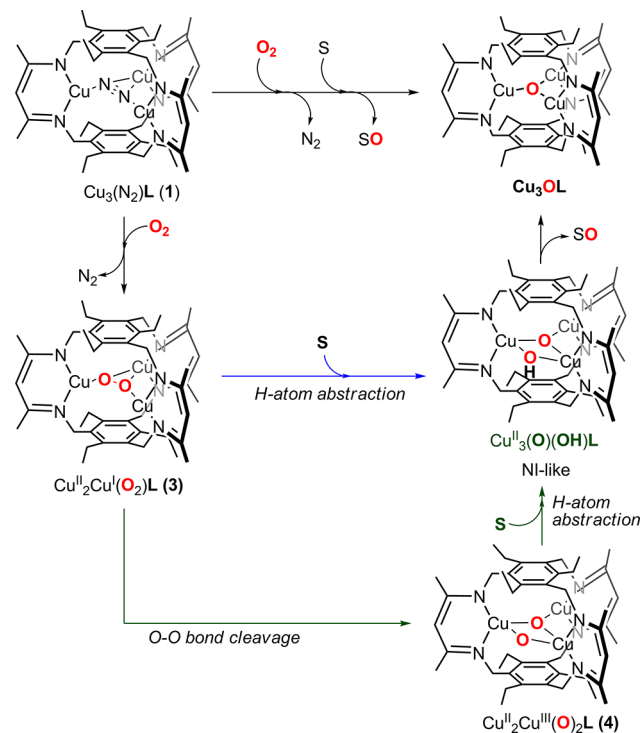
inantly O-centered orbital has out-of-plane p character, indicative of a highly electrophilic O atom. One could, therefore, describe the $[\text{Cu}_3\text{O}_2]^{3+}$ core of $^3\mathbf{4}$ as a (μ -oxyl)(μ_3 -oxo)tricopper(II) species.

To evaluate the mechanism of C–H activation, a toluene molecule was docked into the structure of $^3\mathbf{4}$ near the μ_2 -O atom to afford the stationary point (Figure S51, 4-Tol). Using the maximum along a linear transit for H-abstraction from CH_3 of toluene to the μ_2 -O of $^3\mathbf{4}$ as an initial guess of the transition state (TS), we obtained an optimized TS with $\text{C}\cdots\text{O}$ and $\text{H}\cdots\text{O}$ distances of 2.56 and 1.27 \AA , respectively. This evolves to a (μ -hydroxo)(μ_3 -oxo)tricopper(II) species and a benzyl radical ($5\cdot\text{R}\cdot$, Figure S50). Whereas the μ_2 -O bears radical character resides in an orbital of out-of-plane p -character, the H atom acceptor orbital is of in-plane O $p + \text{Cu } d_{x^2-y^2}$ character and equivalent to orbital 241β in $^3\mathbf{4}$ (Figure S5 and Table S3). Inspection of the molecular orbitals of the TS reveals that electron and proton transfer are simultaneous, consistent with a concerted proton–electron transfer. Subsequent radical rebound is favorable (-33.6 kcal/mol versus $5\cdot\text{R}\cdot$), yielding PhCH_2OH and Cu_3OL (Figure S51). From examination of the two-dimensional (2D) potential energy surface of C–O bond making versus O–Cu bond breaking for this rebound, the step is essentially barrierless (Figure S50), suggesting that accumulation of **5** and benzyl radical dimerization are disfavored.

In our proposed mechanism for O_2 activation and substrate oxidation by **1**, coplanar coordination of O_2 to the Cu_3 centers

results in peroxo- and di(μ -oxo)-tricopper transients, with the former being analogous to PI in MCOs (Scheme 1). The

Scheme 1



perpendicular alignment of the $\text{O}\cdots\text{O}$ vector with respect to the β -diketiminates differs from reported di(μ -oxo)tricopper compounds and decreases metal- O_2 backbonding, which we attribute to the observed reactivity differences.^{6d,8} Although we cannot exclude HAA or hydride abstraction by 3, we note that HAA is rare for peroxo-bridged dicopper complexes and that Et_2O oxidation is not observed despite its lower heterolytic BDE versus PhMe .^{13,31} Importantly, our results parallel O_2 reduction by MCOs, as the μ_2 -oxide is the favored site of formal H atom transfer in both systems, hinting at similar electronic structure in both.³² Whereas NI is protected from reaction with adventitious substrates within the enzyme active site, our NI-like species undergoes a rebound reaction with a previously generated substrate radical.³³

Although dioxygen-copper transients are well-known for HAA, intermolecular O atom transfer coupled to C-H activation remain uncommon. Tricopper complexes facilitate OAT to triphenylphosphine, mediate phenol oxidation, and ligand oxidation.^{7a,d-k,21a,34} Maji et al. reported oxygenated Cu_3 transients competent for acetonitrile hydroxylation and catalytic oxidation of methane, which is the only example of C-H activation by a tricopper system to our knowledge.^{3d,22} We do not observe activation of C-H bonds stronger than that of toluene, suggesting that oxidation of these substrates is not accessible kinetically (e.g., rate of ligand oxidation is competitive). OAT to substrates in both systems is proposed to arise from a di(μ -oxo) tricopper transient, with the μ_2 -O bearing oxyl or oxene character and being the H atom acceptor from substrates. Our system here diverges from that of Chan and co-workers in the reactivity of the μ_3 -O tricopper species. Cu_3OL is reactive toward O_2 with the downstream oxygenated transient being competent for HAA from DHA, whereas that

reported by Chan and co-workers is a terminal unreactive species. This deviation likely originates from the difference in ligand donor strength; the anionic β -diketiminates of our cyclophane afford a more electron-rich tricopper cluster as compared to the neutral donors in Chan's ligand.

Regarding our low yields for OAT to hydrocarbon substrates, we surmise that intramolecular ligand oxidation is competitive with exogenous substrate bond activation. As noted above, the ligand presents four benzylic C-H bonds in the locale for substrate approach. The 2 orders of magnitude increase in product yield with EtSMe as the substrate as compared to toluene or DHA is consistent with our assertion. More pointedly, this increase in yield of the oxidized products leads to a concomitant increase in the formation of Cu_3OL and thereby supports our proposed mechanism; that is, $1\cdot\text{O}_2$, which could be either a peroxo or di(μ -oxo) transient, is indeed the initial active oxidant and not a low-yield minor component in the reaction mixture.

CONCLUSION

In conclusion, we report that $1\cdot\text{O}_2$ transients are competent for OAT to hydrocarbon C-H bonds through an HAA mechanism. Our kinetic, spectroscopic, and DFT analyses are consistent with transient peroxo- and/or di(μ -oxo) species as the likely identity of these reactive species. In addition, the product cluster of OAT, Cu_3OL , is itself reactive toward dioxygen, presenting a unique instance in which the product of a mono-oxygenase reaction retains reactivity toward O_2 . Future studies aim to trap reactive species and enhance ligand stability toward oxidation.

ASSOCIATED CONTENT

Supporting Information

The Supporting Information is available free of charge on the ACS Publications website at DOI: 10.1021/acs.inorgchem.8b00921.

Data from experiments including diode array absorbance changes, ^1H NMR spectra, A_{490} versus time plots, gas chromatograms, mass spectra, ESI/MS spectra, ATR-IR spectra, calculated (TD-DFT) UV-visible spectra, optimized Cartesian coordinates (PDF)

AUTHOR INFORMATION

Corresponding Author

*E-mail: murray@chem.ufl.edu.

ORCID

Matthew T. Kieber-Emmons: 0000-0002-6357-5579

Leslie J. Murray: 0000-0002-1568-958X

Author Contributions

[§]These authors contributed equally.

Notes

The authors declare no competing financial interest.

ACKNOWLEDGMENTS

L.J.M.: Univ. of Florida departmental instrumentation award (NSF CHE-1048604), ACS Petroleum Research Fund (ACS-PRF 52704-DNI3), and NSF CHE-1464876. G.N.D.: Univ. of Florida, College of Liberal Arts and Sciences Graduate Research Fellowship. The content of this publication is solely the responsibility of the authors and does not necessarily represent the official views of NIGMS or NIH. Computational

time was provided by the Extreme Science and Engineering Discovery Environment—supported by NSF ACI-1053575 (TG-CHE130047)—and the Center for High Performance Computing at the Univ. of Utah. The authors thank R. Ferreira (UF), for help collecting ^1H NMR data on **1'**, and Dr. K. M. Light for preliminary calculations.

REFERENCES

- (1) (a) Heppner, D. E.; Kjaergaard, C. H.; Solomon, E. I. Mechanism of the Reduction of the Native Intermediate in the Multicopper Oxidases: Insights into Rapid Intramolecular Electron Transfer in Turnover. *J. Am. Chem. Soc.* **2014**, *136* (51), 17788–17801. (b) Vashchenko, G.; MacGillivray, R. Multi-Copper Oxidases and Human Iron Metabolism. *Nutrients* **2013**, *5*, 2289–2312.
- (2) (a) Chen, Z.; Durão, P.; Silva, C. S.; Pereira, M. M.; Todorovic, S.; Hildebrandt, P.; Bento, I.; Lindley, P. F.; Martins, L. O. The Role of Glu498 in the Dioxygen Reactivity of CotA-laccase from *Bacillus Subtilis*. *Dalton Trans.* **2010**, *39*, 2875–2882. (b) Jolley, R. L., Jr.; Evans, L. H.; Makino, N.; Mason, H. S. Oxytyrosinase. *J. Biol. Chem.* **1974**, *249*, 335–45. (c) Culpepper, M. A.; Rosenzweig, A. C. Architecture and Active Site of Particulate Methane Monooxygenase. *Crit. Rev. Biochem. Mol. Biol.* **2012**, *47*, 483–492. (d) Taylor, A. B.; Stoj, C. S.; Ziegler, L.; Kosman, D. J.; Hart, P. J. The Copper-Iron Connection in Biology: Structure of the Metallo-Oxidase Fet3p. *Proc. Natl. Acad. Sci. U. S. A.* **2005**, *102*, 15459–15464.
- (3) (a) Kakuda, S.; Peterson, R. L.; Ohkubo, K.; Karlin, K. D.; Fukuzumi, S. Enhanced Catalytic Four-Electron Dioxygen (O_2) and Two-Electron Hydrogen Peroxide (H_2O_2) Reduction with a Copper(II) Complex Possessing a Pendant Ligand Pivalamido Group. *J. Am. Chem. Soc.* **2013**, *135* (17), 6513–6522. (b) Dhar, D.; Tolman, W. B. Hydrogen Atom Abstraction from Hydrocarbons by a Copper(III)-Hydroxide Complex. *J. Am. Chem. Soc.* **2015**, *137* (3), 1322–1329. (c) Chan, S. I.; Lu, Y.-J.; Nagababu, P.; Maji, S.; Hung, M.-C.; Lee, M. M.; Hsu, I. J.; Minh, P. D.; Lai, J. C. H.; Ng, K. Y.; Ramalingam, S.; Yu, S. S. F.; Chan, M. K. Efficient Oxidation of Methane to Methanol by Dioxygen Mediated by Tricopper Clusters. *Angew. Chem., Int. Ed.* **2013**, *52* (13), 3731–3735. (d) Glazunova, O. A.; Polyakov, K. M.; Fedorova, T. V.; Dorovatovskii, P. V.; Koroleva, O. V. Elucidation of the Crystal Structure of Corioliopsis Caperata Laccase: Restoration of the Structure and Activity of the Native Enzyme from the T2-depleted Form by Copper Ions. *Acta Crystallogr., Sect. D: Biol. Crystallogr.* **2015**, *71* (4), 854–861.
- (4) Sarangi, R.; Yang, L.; Winikoff, S. G.; Gagliardi, L.; Cramer, C. J.; Tolman, W. B.; Solomon, E. I. X-ray Absorption Spectroscopic and Computational Investigation of a Possible S...S Interaction in the $[\text{Cu}_3\text{S}_2]^{3+}$ Core. *J. Am. Chem. Soc.* **2011**, *133*, 17180–17191.
- (5) (a) Jones, S. M.; Solomon, E. I. Electron transfer and reaction mechanism of laccases. *Cell. Mol. Life Sci.* **2015**, *72* (5), 869–883. (b) Heppner, D. E.; Kjaergaard, C. H.; Solomon, E. I. Molecular Origin of Rapid versus Slow Intramolecular Electron Transfer in the Catalytic Cycle of the Multicopper Oxidases. *J. Am. Chem. Soc.* **2013**, *135* (33), 12212–12215.
- (6) (a) Gupta, A. K.; Tolman, W. B. Cu(I)/O_2 Chemistry Using a β -Diketiminato Supporting Ligand Derived from N,N-Dimethylhydrazine: A $[\text{Cu}_3\text{O}_2]^{3+}$ Complex with Novel Reactivity. *Inorg. Chem.* **2012**, *51*, 1881–1888. (b) Itoh, S.; Nakao, H.; Berreau, L. M.; Kondo, T.; Komatsu, M.; Fukuzumi, S. Mechanistic Studies of Aliphatic Ligand Hydroxylation of a Copper Complex by Dioxygen: A Model Reaction for Copper Monooxygenases. *J. Am. Chem. Soc.* **1998**, *120*, 2890–2899. (c) Itoh, S.; Taki, M.; Nakao, H.; Holland, P. L.; Tolman, W. B.; Que, L., Jr.; Fukuzumi, S. Aliphatic Hydroxylation by a Bis(micro-oxo)dicopper(III) Complex. *Angew. Chem., Int. Ed.* **2000**, *39*, 398–400. (d) Cole, A. P.; Root, D. E.; Mukherjee, P.; Solomon, E. I.; Stack, T. D. A Trinuclear Intermediate in the Copper-Mediated Reduction of O_2 : Four Electrons from Three Coppers. *Science* **1996**, *273*, 1848–50.
- (7) (a) Obias, H. V.; Lin, Y.; Murthy, N. N.; Pidcock, E.; Solomon, E. I.; Ralle, M.; Blackburn, N. J.; Neuhold, Y.-M.; Zuberbühler, A. D.; Karlin, K. D. Peroxo-, Oxo-, and Hydroxo-Bridged Dicopper Complexes: Observation of Exogenous Hydrocarbon Substrate Oxidation. *J. Am. Chem. Soc.* **1998**, *120* (49), 12960–12961. (b) Mahapatra, S.; Halfen, J. A.; Wilkinson, E. C.; Que, L.; Tolman, W. B. Modeling Copper-Dioxygen Reactivity in Proteins: Aliphatic C-H Bond Activation by a New Dicopper(II)-Peroxo Complex. *J. Am. Chem. Soc.* **1994**, *116* (21), 9785–9786. (c) Pidcock, E.; DeBeer, S.; Obias, H. V.; Hedman, B.; Hodgson, K. O.; Karlin, K. D.; Solomon, E. I. A Study of Solid $[\{\text{Cu}(\text{MePY}_2)\}_2\text{O}_2]^{2+}$ Using Resonance Raman and X-ray Absorption Spectroscopies: An Intermediate Cu_2O_2 Core Structure or a Solid Solution? *J. Am. Chem. Soc.* **1999**, *121* (9), 1870–1878. (d) Citek, C.; Herres-Pawlis, S.; Stack, T. D. P. Low Temperature Syntheses and Reactivity of Cu_2O_2 Active-Site Models. *Acc. Chem. Res.* **2015**, *48* (8), 2424–2433. (e) Kang, P.; Bobyr, E.; Dustman, J.; Hodgson, K. O.; Hedman, B.; Solomon, E. I.; Stack, T. D. P. Bis(μ -oxo) Dicopper(III) Species of the Simplest Peralkylated Diamine: Enhanced Reactivity toward Exogenous Substrates. *Inorg. Chem.* **2010**, *49* (23), 11030–11038. (f) Matsumoto, T.; Furutachi, H.; Kobino, M.; Tomii, M.; Nagatomo, S.; Tosha, T.; Osako, T.; Fujinami, S.; Itoh, S.; Kitagawa, T.; Suzuki, M. Intramolecular Arene Hydroxylation versus Intermolecular Olefin Epoxidation by $(\mu\text{-}\eta^2\text{-}\eta^2\text{-Peroxo})\text{dicopper(II)}$ Complex Supported by Dinucleating Ligand. *J. Am. Chem. Soc.* **2006**, *128* (12), 3874–3875. (g) Lucas, H. R.; Li, L.; Sarjeant, A. A. N.; Vance, M. A.; Solomon, E. I.; Karlin, K. D. Toluene and Ethylbenzene Aliphatic C-H Bond Oxidations Initiated by a Dicopper(II)- μ -1,2-Peroxo Complex. *J. Am. Chem. Soc.* **2009**, *131* (9), 3230–3245. (h) Matsumoto, T.; Ohkubo, K.; Honda, K.; Yazawa, A.; Furutachi, H.; Fujinami, S.; Fukuzumi, S.; Suzuki, M. Aliphatic C-H Bond Activation Initiated by a $(\mu\text{-}\eta^2\text{-}\eta^2\text{-Peroxo})\text{dicopper(II)}$ Complex in Comparison with Cumylperoxyl Radical. *J. Am. Chem. Soc.* **2009**, *131* (26), 9258–9267. (i) Blackburn, N. J.; Karlin, K. D.; Concannon, M.; Hayes, J. C.; Gultneh, Y.; Zubieta, J. Studies on a Model Copper Mono-Oxygenase System: Peroxo-Cu Binuclear Intermediates in the Hydroxylation of an Aromatic Ring. *J. Chem. Soc., Chem. Commun.* **1984**, *14*, 939–940. (j) Halfen, J. A.; Young, V. G.; Tolman, W. B. Dioxygen Activation by a Copper(I) Complex of a New Tetradentate Tripodal Ligand: Mechanistic Insights into Peroxodicopper Core Reactivity. *J. Am. Chem. Soc.* **1996**, *118* (44), 10920–10921. (k) Sanyal, I.; Mahroof-Tahir, M.; Nasir, M. S.; Ghosh, P.; Cohen, B. I.; Gultneh, Y.; Cruse, R. W.; Farooq, A.; Karlin, K. D. Reactions of Dioxygen (O_2) with Mononuclear Copper(I) Complexes: Temperature-Dependent Formation of Oeroxo- or oxo- (and dihydroxo-) Bridged Dicopper(II) Complexes. *Inorg. Chem.* **1992**, *31* (21), 4322–4332.
- (8) Nechaev, M. S.; Rayón, V. M.; Frenking, G. Energy Partitioning Analysis of the Bonding in Ethylene and Acetylene Complexes of Group 6, 8, and 11 Metals: $(\text{CO})_5\text{TM}-\text{C}_2\text{H}_4$ and $\text{Cl}_4\text{TM}-\text{C}_2\text{H}_4$ ($\text{TM} = \text{Cr}, \text{Mo}, \text{W}$), $(\text{CO})_4\text{TM}-\text{C}_2\text{H}_4$ ($\text{TM} = \text{Fe}, \text{Ru}, \text{Os}$), and $\text{TM}^+-\text{C}_2\text{H}_4$ ($\text{TM} = \text{Cu}, \text{Ag}, \text{Au}$). *J. Phys. Chem. A* **2004**, *108* (15), 3134–3142.
- (9) (a) Di Francesco, G. N.; Gaillard, A.; Ghiviriga, I.; Abboud, K. A.; Murray, L. J. Modeling Biological Copper Clusters: Synthesis of a Tricopper Complex, and Its Chloride- and Sulfide-Bridged Congeners. *Inorg. Chem.* **2014**, *53* (9), 4647–4654. (b) Murray, L. J.; Weare, W. W.; Shearer, J.; Mitchell, A. D.; Abboud, K. A. Isolation of a (Dinitrogen)Tricopper(I) Complex. *J. Am. Chem. Soc.* **2014**, *136* (39), 13502–13505. (c) Guillet, G. L.; Sloane, F. T.; Ermert, D. M.; Calkins, M. W.; Peprah, M. K.; Knowles, E. S.; Čížmár, E.; Abboud, K. A.; Meisel, M. W.; Murray, L. J. Preorganized Assembly of Three Iron(II) or Manganese(II) β -diketiminato Complexes Using a Cyclophane Ligand. *Chem. Commun.* **2013**, *49* (59), 6635–6637.
- (10) Armarego, W. L. F.; Chai, C. L. L. Common Physical Techniques Used in Purification. In *Purification of Laboratory Chemicals*, 6th ed.; Butterworth-Heinemann: Oxford, England, 2009; pp 1–60.
- (11) Favier, I.; Duñach, E. New Protic Salts of Aprotic Polar Solvents. *Tetrahedron Lett.* **2004**, *45* (17), 3393–3395.
- (12) (a) Sastri, C. V.; Lee, J.; Oh, K.; Lee, Y. J.; Lee, J.; Jackson, T. A.; Ray, K.; Hirao, H.; Shin, W.; Halfen, J. A.; Kim, J.; Que, L.; Shaik, S.; Nam, W. Axial Ligand Tuning of a Nonheme Iron(IV)–oxo Unit for Hydrogen Atom Abstraction. *Proc. Natl. Acad. Sci. U. S. A.* **2007**, *104* (49), 19181–19186. (b) Lee, Y.; Sloane, F. T.; Blondin, G.; Abboud, K. A.; García-Serres, R.; Murray, L. J. Dinitrogen Activation Upon

Reduction of a Triiron(II) Complex. *Angew. Chem.* **2015**, *127* (5), 1519–1523.

(13) Beauvais, L. G.; Lippard, S. J. Reactions of the Peroxo Intermediate of Soluble Methane Monooxygenase Hydroxylase with Ethers. *J. Am. Chem. Soc.* **2005**, *127* (20), 7370–7378.

(14) Garcia-Bosch, I.; Company, A.; Frisch, J. R.; Torrent-Sucarrat, M.; Cardellach, M.; Gamba, I.; Güell, M.; Casella, L.; Que, L.; Ribas, X.; Luis, J. M.; Costas, M. O₂ Activation and Selective Phenolate ortho Hydroxylation by an Unsymmetric Dicopper μ - η^1 : η^1 -Peroxo Complex. *Angew. Chem., Int. Ed.* **2010**, *49* (13), 2406–2409.

(15) Frisch, M. J.; Trucks, G. W.; Schlegel, H. B.; Scuseria, G. E.; Robb, M. A.; Cheeseman, J. R.; Scalmani, G.; Barone, V.; Petersson, G. A.; Nakatsuji, H.; Li, X.; Caricato, M.; Marenich, A. V.; Bloino, J.; Janesko, B. G.; Gomperts, R.; Mennucci, B.; Hratchian, H. P.; Ortiz, J. V.; Izmaylov, A. F.; Sonnenberg, J. L.; Williams, Ding, F.; Lipparini, F.; Egidi, F.; Goings, J.; Peng, B.; Petrone, A.; Henderson, T.; Ranasinghe, D.; Zakrzewski, V. G.; Gao, J.; Rega, N.; Zheng, G.; Liang, W.; Hada, M.; Ehara, M.; Toyota, K.; Fukuda, R.; Hasegawa, J.; Ishida, M.; Nakajima, T.; Honda, Y.; Kitao, O.; Nakai, H.; Vreven, T.; Throssell, K.; Montgomery, J. A., Jr.; Peralta, J. E.; Ogliaro, F.; Bearpark, M. J.; Heyd, J. J.; Brothers, E. N.; Kudin, K. N.; Staroverov, V. N.; Keith, T. A.; Kobayashi, R.; Normand, J.; Raghavachari, K.; Rendell, A. P.; Burant, J. C.; Iyengar, S. S.; Tomasi, J.; Cossi, M.; Millam, J. M.; Klene, M.; Adamo, C.; Cammi, R.; Ochterski, J. W.; Martin, R. L.; Morokuma, K.; Farkas, O.; Foresman, J. B.; Fox, D. J. *Gaussian 16*; Gaussian, Inc: Wallingford, CT, 2016.

(16) Schäfer, A.; Huber, C.; Ahlrichs, R. Fully Optimized Contracted Gaussian Basis Sets of Triple Zeta Valence Quality for Atoms Li to Kr. *J. Chem. Phys.* **1994**, *100* (8), 5829–5835.

(17) Schäfer, A.; Horn, H.; Ahlrichs, R. Fully Optimized Contracted Gaussian Basis Sets for Atoms Li to Kr. *J. Chem. Phys.* **1992**, *97* (4), 2571–2577.

(18) Stephens, P. J.; Devlin, F. J.; Chabalowski, C. F.; Frisch, M. J. Ab Initio Calculation of Vibrational Absorption and Circular Dichroism Spectra Using Density Functional Force Fields. *J. Phys. Chem.* **1994**, *98* (45), 11623–11627.

(19) Tenderholt, A. L. *QMForge, Version 2.1*; Stanford University: Stanford, CA, 2007.

(20) Kieber-Emmons, M. T. *Lumo*, 1.3; Kieber-Emmons, Matthew T.: Salt Lake City, UT, 2013.

(21) (a) Lewis, E. A.; Tolman, W. B. Reactivity of Dioxxygen–Copper Systems. *Chem. Rev.* **2004**, *104* (2), 1047–1076. (b) Elwell, C. E.; Gagnon, N. L.; Neisen, B. D.; Dhar, D.; Spaeth, A. D.; Yee, G. M.; Tolman, W. B. Copper–Oxygen Complexes Revisited: Structures, Spectroscopy, and Reactivity. *Chem. Rev.* **2017**, *117* (3), 2059–2107. (c) Dalle, K. E.; Gruene, T.; Dechert, S.; Demeshko, S.; Meyer, F. Weakly Coupled Biologically Relevant Cu^{II}(μ - η^1 : η^1 -O₂) cis-Peroxo Adduct that Binds Side-On to Additional Metal Ions. *J. Am. Chem. Soc.* **2014**, *136* (20), 7428–7434. (d) Kindermann, N.; Bill, E.; Dechert, S.; Demeshko, S.; Reijerse, E. J.; Meyer, F. A Ferromagnetically Coupled (S = 1) Peroxodicopper(II) Complex. *Angew. Chem., Int. Ed.* **2015**, *54* (6), 1738–1743.

(22) Maji, S.; Lee, J. C. M.; Lu, Y.-J.; Chen, C.-L.; Hung, M.-C.; Chen, P. P. Y.; Yu, S. S. F.; Chan, S. I. Dioxxygen Activation of a Trinuclear Cu^ICu^ICu^I Cluster Capable of Mediating Facile Oxidation of Organic Substrates: Competition between O-Atom Transfer and Abortive Intercomplex Reduction. *Chem. - Eur. J.* **2012**, *18* (13), 3955–3968.

(23) Solomon, E. I.; Heppner, D. E.; Johnston, E. M.; Ginsbach, J. W.; Cirera, J.; Qayyum, M.; Kieber-Emmons, M. T.; Kjaergaard, C. H.; Hadt, R. G.; Tian, L. Copper Active Sites in Biology. *Chem. Rev.* **2014**, *114* (7), 3659–3853.

(24) Yoon, J.; Solomon, E. I. Electronic Structure of the Peroxy Intermediate and Its Correlation to the Native Intermediate in the Multicopper Oxidases: Insights into the Reductive Cleavage of the O–O Bond. *J. Am. Chem. Soc.* **2007**, *129* (43), 13127–13136.

(25) (a) Machonkin, T. E.; Mukherjee, P.; Henson, M. J.; Stack, T. D. P.; Solomon, E. I. The EPR Spectrum of a Cu(II/II/III) Cluster: Anisotropic Exchange in a Bent Cu(II)₂O₂ core. *Inorg. Chim. Acta*

2002, *341*, 39–44. (b) Kindermann, N.; Dechert, S.; Demeshko, S.; Meyer, F. Proton-Induced, Reversible Interconversion of a μ -1,2-Peroxo and a μ -1,1-Hydroperoxo Dicopper(II) Complex. *J. Am. Chem. Soc.* **2015**, *137* (25), 8002–8005.

(26) Garcia-Bosch, I.; Cowley, R. E.; Díaz, D. E.; Siegler, M. A.; Nam, W.; Solomon, E. I.; Karlin, K. D. Dioxxygen Activation by a Macrocyclic Copper Complex Leads to a Cu₂O₂ Core with Unexpected Structure and Reactivity. *Chem. - Eur. J.* **2016**, *22* (15), 5133–5137.

(27) Chan, S. I.; Chien, C. Y. C.; Yu, C. S. C.; Nagababu, P.; Maji, S.; Chen, P. P. Y. Efficient Catalytic Oxidation of Hydrocarbons Mediated by Tricopper Clusters Under Mild Conditions. *J. Catal.* **2012**, *293*, 186–194.

(28) (a) Nam, W. High-Valent Iron(IV)–Oxo Complexes of Heme and Non-Heme Ligands in Oxygenation Reactions. *Acc. Chem. Res.* **2007**, *40* (7), 522–531. (b) Hong, S.; Lee, Y.-M.; Cho, K.-B.; Sundaravel, K.; Cho, J.; Kim, M. J.; Shin, W.; Nam, W. Ligand Topology Effect on the Reactivity of a Mononuclear Nonheme Iron(IV)–Oxo Complex in Oxygenation Reactions. *J. Am. Chem. Soc.* **2011**, *133* (31), 11876–11879.

(29) Pratt, D. A.; Mills, J. H.; Porter, N. A. Theoretical Calculations of Carbon–Oxygen Bond Dissociation Enthalpies of Peroxyl Radicals Formed in the Autoxidation of Lipids. *J. Am. Chem. Soc.* **2003**, *125* (19), 5801–5810.

(30) (a) Halfen, J. A.; Mahapatra, S.; Wilkinson, E. C.; Kaderli, S.; Young, V. G.; Que, L.; Zuberbühler, A. D.; Tolman, W. B. Reversible Cleavage and Formation of the Dioxxygen O–O Bond Within a Dicopper Complex. *Science* **1996**, *271* (5254), 1397–1400. (b) Cramer, C. J.; Wloch, M.; Piecuch, P.; Puzzarini, C.; Gagliardi, L. Theoretical Models on the Cu₂O₂ Torture Track: Mechanistic Implications for Oxytyrosinase and Small-Molecule Analogues. *J. Phys. Chem. A* **2006**, *110* (5), 1991–2004.

(31) (a) Baik, M.-H.; Newcomb, M.; Friesner, R. A.; Lippard, S. J. Mechanistic Studies on the Hydroxylation of Methane by Methane Monooxygenase. *Chem. Rev.* **2003**, *103* (6), 2385–2420. (b) Valentine, A. M.; Stahl, S. S.; Lippard, S. J. Mechanistic Studies of the Reaction of Reduced Methane Monooxygenase Hydroxylase with Dioxxygen and Substrates. *J. Am. Chem. Soc.* **1999**, *121* (16), 3876–3887. (c) Jiang, Y.; Wilkins, P. C.; Dalton, H. Activation of the Hydroxylase of sMMO from *Methylococcus Capsulatus* (Bath) by Hydrogen peroxide. *Biochim. Biophys. Acta, Protein Struct. Mol. Enzymol.* **1993**, *1163* (1), 105–112.

(32) (a) Halle, L. F.; Klein, F. S.; Beauchamp, J. L. Properties and Reactions of Organometallic Fragments in the Gas Phase. Ion Beam Studies of Hydridoiron(1+) ion. *J. Am. Chem. Soc.* **1984**, *106* (9), 2543–2549. (b) Screttas, C. G. Some Properties of Heterolytic Bond Dissociation Energies and Their use as Molecular Parameters for Rationalizing or Predicting Reactivity. *J. Org. Chem.* **1980**, *45* (2), 333–336.

(33) Lockwood, M. A.; Wang, K.; Mayer, J. M. Oxidation of Toluene by [(phen)₂Mn(μ -O)₂Mn(phen)₂]⁴⁺ via Initial Hydride Abstraction. *J. Am. Chem. Soc.* **1999**, *121* (50), 11894–11895.

(34) (a) Lionetti, D.; Day, M. W.; Agapie, T. Metal-Templated Ligand Architectures for Trinuclear Chemistry: Tricopper Complexes and Their O₂ Reactivity. *Chem. Sci.* **2013**, *4* (2), 785–790. (b) Paul, P. P.; Tyeklár, Z.; Jacobson, R. R.; Karlin, K. D. Reactivity Patterns and Comparisons in Three Classes of Synthetic Copper-Dioxxygen {Cu₂-O₂} Complexes: Implication for Structure and Biological Relevance. *J. Am. Chem. Soc.* **1991**, *113* (14), 5322–5332.

(35) Cook, B. J.; Di Francesco, G. N.; Ferreira, R. B.; Lukens, J. T.; Silberstein, K. E.; Keegan, B. C.; Catalano, V. J.; Lancaster, K. M.; Shearer, J.; Murray, L. J. Chalcogen Impact on Covalency within Molecular [Cu₃(μ_3 -E)]³⁺ Clusters (E = O, S, Se): A Synthetic, Spectroscopic, and Computational Study. *Manuscript Under Revision*. **2018**.